

# Numerical study on the validity of the diffusion approximation for computational optical biopsy

Haiou Shen, WenXiang Cong, Xin Qian, Kumar Durairaj, and Ge Wang

*Department of Radiology, University of Iowa, Iowa City, Iowa 52242*

Received April 5, 2006; revised August 23, 2006; accepted August 24, 2006;  
posted September 6, 2006 (Doc. ID 69654); published January 10, 2007

Currently, we are developing a computational optical biopsy technology for molecular sensing. We use the diffusion equation to model photon propagation but have a concern about the accuracy of diffusion approximation when the optical sensor is close to a bioluminescent source. We derive formulas to describe photon fluence for point and ball sources and measurement formulas for an idealized optical biopsy probe. Then, we numerically compare the diffusion approximation and the radiative transport as implemented by Monte Carlo simulation in the cases of point and ball sources. Our simulation results show that the diffusion approximation can be accurately applied if  $\mu'_s \gg \mu_a$  even if the sensor is very close to the source ( $>1$  mm). Furthermore, an approximate formula is given to describe the measurement of a cut-end fiber probe for a ball source. © 2007 Optical Society of America

OCIS codes: 170.3660, 290.1990, 170.6280.

## 1. INTRODUCTION

The use of optical probes (fluorescence and bioluminescence) to depict gene expression and other molecular signatures *in vitro* is a well-established technique for biological studies and has been recently extended into living small animal models. Optical molecular tomography, namely, bioluminescence tomography<sup>1–5</sup> (BLT) and fluorescence molecular tomography (FMT),<sup>6</sup> is a rapidly developing area of optical molecular imaging. One major obstacle for optical molecular tomography is that when light sources are small, weak, and deep in a living body, they cannot be effectively imaged because of the strong absorption and scattering in tissues. The problem is more serious with larger animals and in clinical settings.

We have proposed a computational optical biopsy (COB) approach<sup>7,8</sup> to meet this challenge. The COB is to localize and quantify light sources *in vivo* deep inside a living animal or patient. The key components of a COB system are an optical probe such as a fiber-based needle, a data acquisition unit, and a computational engine. The data collected by the probe along one or multiple trajectories are processed to estimate the source parameters of interest. Optical properties of the tissues and organs may also be recovered in the COB process to facilitate the recovery of the source features.

Biological tissue is a turbid medium that both scatters and absorbs photons. The propagation of photons can be accurately modeled by the radiative transport equation (RTE).<sup>9,10</sup> Because of the difficulties in handling the RTE directly, the diffusion approximation to the transport equation has been widely used in biophotonics.<sup>11–15</sup> To apply the diffusion approximation, photon scattering must be the dominant factor in the material.<sup>16</sup> Most applications of the diffusion approximation are with large propa-

gation distance<sup>17,18</sup> in order for the weakly anisotropic light propagation assumption to hold. In biological tissue, photons are scattered due to changes in the refractive index at cell membranes and internal organelles. Typically, for  $\lambda > 600$  nm, the effective scattering coefficient is much stronger than the absorption coefficient for biological tissues.<sup>19,20</sup> The firefly luciferase for bioluminescence has a broad spectrum and contains a large component above 600 nm.<sup>21</sup> In fact, for BLT, we have used the diffusion theory to describe the bioluminescent light transportation in tissue. For BLT, the measurement is on the surface. The distance between the bioluminescent source and the surface generally is large enough to support the weakly anisotropic light propagation assumption.

In our proposed COB, an optical fiber-based probe is inserted into the tissue to be near or even inside a bioluminescent light source to collect the light signal. Therefore, the critical important question that arises is, “Can we apply the diffusion approximation for COB?” Flock *et al.*<sup>22</sup> simulated an infinitesimally wide (pencil) beam normally incident on a homogeneous semi-infinite slab and compared the results with the diffusion theory for photon fluence and showed that the diffusion approximation is accurate for weakly anisotropic light propagation and high values of the scattering albedo. But their result does not answer our question. Since there is no prior work targeting this question, here we employ the Monte Carlo simulation<sup>23</sup> to study the validity of the diffusion equation in the COB context with an emphasis on bioluminescence-based COB. In Section 2, we present several diffusion formulas for point and ball sources. In Section 3, we compare the Monte Carlo simulation and the diffusion approximation. Finally, in Section 4, we discuss relevant issues and conclude the paper.

## 2. DIFFUSION-APPROXIMATION-BASED FORMULAS

Biological tissue is a turbid medium that both scatters and absorbs photons. The three key parameters to describe scattering and absorption are absorption coefficient  $\mu_a$  ( $\text{cm}^{-1}$ ), scattering coefficient  $\mu_s$  ( $\text{cm}^{-1}$ ), and anisotropy  $g$ .  $\mu_a$  is defined as the probability of photon absorption per unit infinitesimal path length, and  $\mu_s$  is the probability of scattering per unit infinitesimal path length.  $g$  is the average of the cosine value of the deflection angle.

COB<sup>8</sup> is used to localize and quantify a light source deep inside a subject. In contrast to existing optical biopsy methods, this scheme is used to collect optical signals directly from a region of interest along one or several biopsy injection paths in a subject, and then compute features of an underlying light source distribution. In COB, since the detector is deep inside the medium, in its local neighborhood, the boundary condition has almost no effect. Hence, we can assume that the medium is infinite. The shape of a real bioluminescent source is irregular, but given the strong scattering, a ball source assumption is a good starting point. In the following, we will assume an infinite homogeneous medium embedded with a point or ball source.

Two types of optical fibers can be used to collect optical signals: an isotropic optical probe (a ruby sphere glued on the tip of a cut-end fiber) can be used to measure the local fluence rate and a cut-end fiber can be used to measure the incident photons on the cut-end tip. In the case of a homogeneous tissue with  $\mu_a \ll \mu_s$ , a diffusion formula has been widely used to describe the photon transport. Figure 1 shows a point source and a ball source. With a point source, the photon fluence  $\phi_P^F$  ( $\text{W}/\text{cm}^2$ ) decays exponentially according to<sup>11</sup>

$$\phi_P^F(\hat{r}) = \frac{Pe^{-\mu_{\text{eff}}r}}{4\pi Dr}, \quad (1)$$

where  $P$  is the source power,  $D$  is the diffusion coefficient defined by  $D=1/[3(\mu'_s + \mu_a)]$  (cm), and  $\mu_{\text{eff}}=[3\mu_a(\mu'_s + \mu_a)]^{1/2}$  ( $\text{cm}^{-1}$ ),  $\mu'_s=(1-g)\mu_s$  ( $\text{cm}^{-1}$ ) is referred to as the reduced scattering coefficient ( $\text{cm}^{-1}$ ). The scattering angle in the tissue is usually small with  $g \approx 0.9$ . Note that the Euclidean norm of a vector  $\hat{v}$  is represented as  $v$ . In this formula,  $\hat{r}$  is the vector from the detector to the light source,  $r$  is the Euclidean norm of  $\hat{r}$ . In our simulation experiments, the number of photons per second is used for the measurement of the power.

Then, we derive the following two formulas to describe the photon fluence from a ball source:

$$\begin{aligned} \phi_{B,r \geq R}^F(\hat{r}, R) &= \phi_P^F(\hat{r}) \frac{3[(e^{-R\mu_{\text{eff}}} - e^{R\mu_{\text{eff}}}) + R\mu_{\text{eff}}(e^{-R\mu_{\text{eff}}} + e^{R\mu_{\text{eff}}})]}{2R^3\mu_{\text{eff}}^3}, \quad (2a) \end{aligned}$$

$$\begin{aligned} \phi_{B,r < R}^F(\hat{r}, R) &= \phi_P^F(\hat{r}) \frac{3e^{-R\mu_{\text{eff}}}\{1 - e^{2r\mu_{\text{eff}}} + [2e^{(r+R)\mu_{\text{eff}}}r + R - e^{2r\mu_{\text{eff}}}R]\mu_{\text{eff}}\}}{2R^3\mu_{\text{eff}}^3}. \quad (2b) \end{aligned}$$

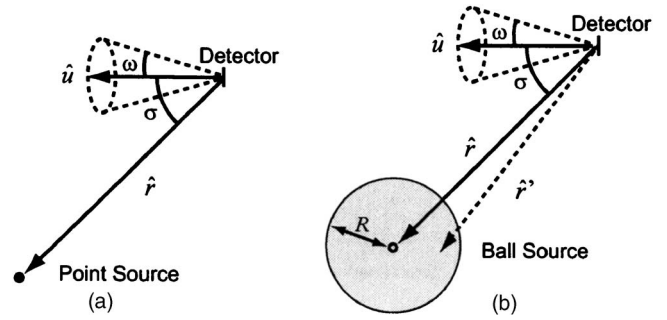


Fig. 1. Illustration of the point and ball source models.  $\hat{r}$  is the vector from the center of the detector to the source,  $\hat{u}$  is the unit normal vector of the detector surface,  $\omega$  is the half-angle of the cone that indicates the maximum incident angle of photons intercepted by the detector,  $\sigma$  is the angle between  $\hat{r}$  and  $\hat{u}$ , and  $R$  is the radius of the ball source. (a) Point source. (b) Solid ball source.

These formulas are derived from Eq. (1) after an integration over the region of the ball source. Equation (2a) can also be derived using Green's function.<sup>24</sup> As shown in Fig. 1(b),  $R$  is the radius of the ball source. If  $r \geq R$ , the difference between a ball source and a point source is a multiplicative constant, which relies only on  $R$  and  $\mu_{\text{eff}}$ . It may appear that if  $r \gg R$ , then a ball source will be equivalent to a point source of the same total power. However, as shown below in our simulation, the ratio between the photon fluence measures due to a ball source and a point source is indeed very close to the constant predicted by Eq. (2a).

Even using an isotropic probe, photon fluence is not easy to measure in practice. In our COB configuration, a cut-end fiber is employed. In this case, we need a formula to describe the number of detectable photons incident on a unit plane detector surface. For that purpose, the radiance  $L$  ( $\text{W}/\text{cm}^2/\text{sr}$ ) in a tissue along a unit vector  $\hat{s}$  is given by<sup>25</sup>

$$L(\hat{r}, \hat{s}) = \frac{1}{4\pi} [\phi_P^F(\hat{r}) + 3j(\hat{r}) \cdot \hat{s}], \quad (3)$$

where  $j(\hat{r})$  is the flux, which is related to the fluence through  $j(\hat{r}) = -D\nabla\phi_P^F(\hat{r})$ .

Based on the radiance, we can describe the detector measurement. For a point source, we have

$$\begin{aligned} \phi_P^M(\hat{r}, \hat{u}, \omega) &= \phi_P^F(\hat{r}) \frac{r \sin(\omega)^2 + 2D \cos(\sigma)[1 - \cos(\omega)^3](1 + r\mu_{\text{eff}})}{4r}. \quad (4) \end{aligned}$$

As shown in Fig. 1(a),  $\hat{u}$  is the unit normal vector of the detector surface,  $\omega$  is the half-angle of the cone, which indicates the maximum incident angle of photons intercepted by the detector,  $\cos(\sigma) = \hat{r} \cdot \hat{u} / ru$ . The number of the detected photons can be calculated as  $\phi_P^M \times S$ , where  $S$  is the area of the detector.

For a solid ball source, we can have the following integration formula based on Eq. (4),

$$\phi_B^M(\hat{r}, \hat{u}, \omega, R) = \oint_{\Omega} \phi_P^M(\hat{r}', \hat{u}, \omega) d\Omega, \quad (5)$$

where  $\Omega$  is the region of the ball. There are numerous ways to compute this integration. Our way is to use the Monte Carlo integration<sup>23</sup> that gives satisfactory results efficiently. In the next section, based on our simulation results, we have derived an approximation formula for Eq. (5).

### 3. NUMERICAL SIMULATION RESULTS

In this section, we will verify the above formulas by Monte Carlo simulation in the COB context. The Monte Carlo method<sup>23</sup> is a good standard technique to solve complex biophotonic problems.<sup>22,26–30</sup> MCML<sup>29</sup> is one of the state-of-the-art Monte Carlo simulation program, which simulates the light transportation in multilayered tissues. Our situation is different where a point or ball source is embedded in an infinite medium, which can be homogeneous or radially heterogeneous. Based on MCML, we developed a Monte Carlo simulation program. The accuracy of the code was verified by extensive comparison with another open-source Monte Carlo program<sup>31</sup> and a commercial program: TracePro (Lambda Research Corp.).

In our program, we use the same formulas as in the MCML to define the photon launching, step size, photon

absorption, and photon scattering. As shown in Fig. 2, a point or ball source is inside the medium, and a set of concentric shells around the source is generated with a 0.01 cm thickness between adjacent shells. A variable “Absorption” is associated with each shell. If some energy is lost in a shell, the lost energy will be added to the Absorption of this shell. The absorbed photon energy can be converted into the photon fluence  $\phi^F(\hat{r})$ , which is equal to the energy divided by the coefficient  $\mu_a$ . Using this technique, Eqs. (1) and (2) can be evaluated for accuracy.

To verify Eq. (4), which presents the measurement with a detector, we considered a special case:

$$\phi_{\text{Point}}^M(\hat{r}, \hat{u}, \pi/2) = \phi_{\text{Point}}^F(\hat{r}) \frac{r + 2D(1 + r\mu_{\text{eff}})}{4r}. \quad (6)$$

In this formula, the detector surface is oriented toward the light source directly,  $\cos(\sigma)=1$ , and the numerical ap-

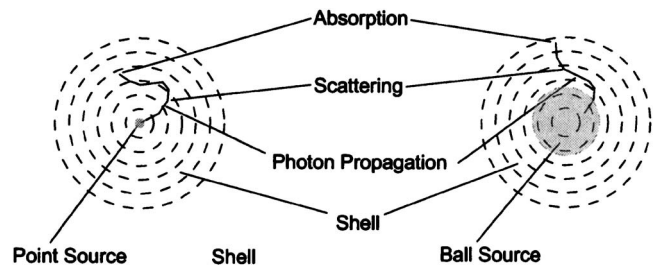


Fig. 2. Illustration of the Monte Carlo simulation of the point and ball sources in an infinite medium.

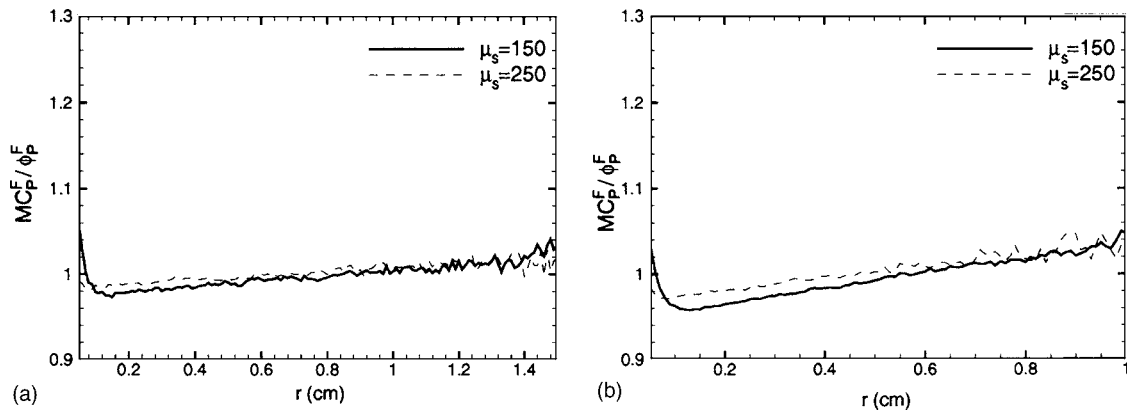


Fig. 3. Comparison of  $MC_P^F$  and  $\phi_P^F$  [Eq. (1)] for a point source in an infinite medium with  $g=0.9$  and  $\mu_s=\{50,150,250\}$  ( $\text{cm}^{-1}$ ). (a)  $\mu_a=0.2$  ( $\text{cm}^{-1}$ ), (b)  $\mu_a=0.5$  ( $\text{cm}^{-1}$ ), (c)  $\mu_a=1.0$  ( $\text{cm}^{-1}$ ), (d)  $\mu_a=2.0$  ( $\text{cm}^{-1}$ ).

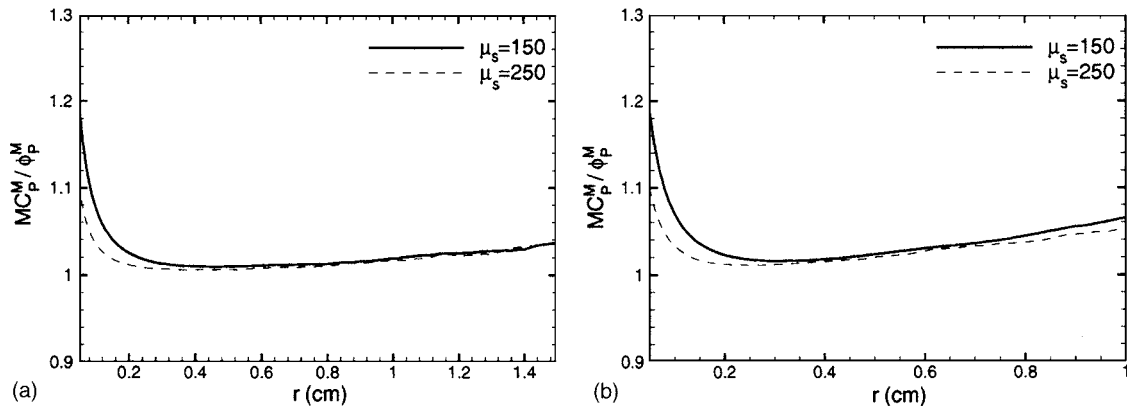


Fig. 4. Comparison of  $MC_P^M$  and  $\phi_P^M$  [Eq. (4)] for a point source in an infinite medium with  $g=0.9$  and  $\mu_s=\{50,150,250\}$  ( $\text{cm}^{-1}$ ). (a)  $\mu_a=0.2$  ( $\text{cm}^{-1}$ ), (b)  $\mu_a=0.5$  ( $\text{cm}^{-1}$ ), (c)  $\mu_a=1.0$  ( $\text{cm}^{-1}$ ), (d)  $\mu_a=2.0$  ( $\text{cm}^{-1}$ ).

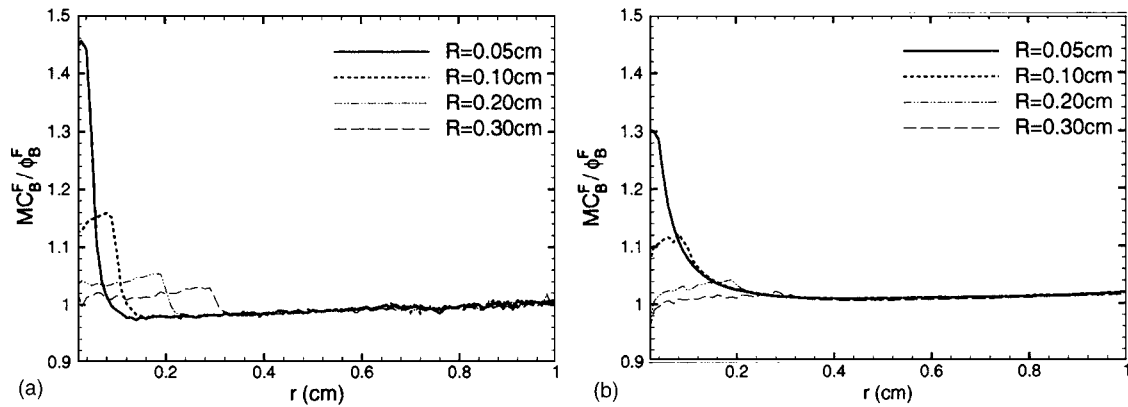


Fig. 5. (a) Comparison of  $MC_B^F$  and  $\phi_B^F$  [Eq. (2)] and (b) comparison of  $MC_B^M$  and  $\phi_B^M$  [Eq. (5)] with  $\mu_a=0.5$ ,  $\mu_s=150$ , and  $g=0.9$  for different  $R=\{0.05, 0.1, 0.2, 0.3\}$  cm.

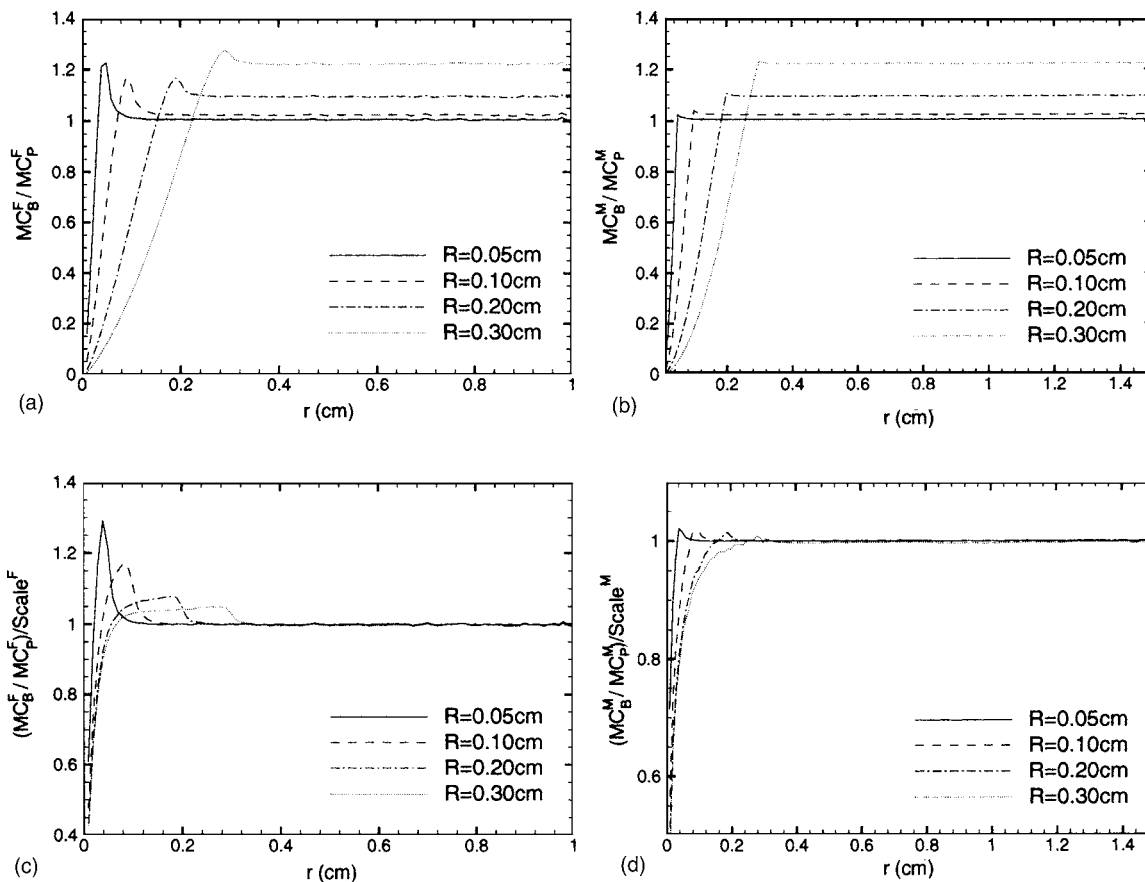


Fig. 6. (a) Comparison of  $MC_B^F$  and  $MC_P^F$ ; (b) comparison of  $MC_B^M$  and  $MC_P^M$ ; (c) comparison of  $MC_B^F/MC_P^F$  and the diffusion prediction  $scale^F$ ; (d) comparison of  $MC_B^M/MC_P^M$  and the diffusion prediction  $scale^M$ .  $\mu_a=0.5$ ,  $\mu_s=150$ , and  $g=0.9$  for different  $R=\{0.05, 0.1, 0.2, 0.3\}$  cm. (a) and (b) show that  $MC_B^F/MC_P^F$  and  $MC_B^M/MC_P^M$  are constant for  $r>R$ . (c) and (d) show that  $MC_B^F/MC_P^F \approx scale^F$  and  $MC_B^M/MC_P^M \approx scale^M$  for  $r>R$ .

erture  $\sin(\pi/2)=1$ . In this study, we assumed that the size of the detector was  $0.02^2 \pi$  ( $\text{cm}^2$ ). Then, for each shell, another variable, “OutPhotons,” is also utilized. In the Monte Carlo simulation, the program recorded the number of photons that traveled from one shell to an immediate outer shell in the variable OutPhotons. Using this technique, we can verify Eq. (6). Alternatively, a plane detector was placed in the medium to record the number of photons incident on its surface to verify Eq. (6). Most Monte Carlo simulation programs allow one to equiva-

lently propagate many photons as a packet along a particular pathway simultaneously to improve the efficiency of the simulation.<sup>29</sup> Another old way is to set one photon for each packet, which can improve the simulation accuracy. In our Monte Carlo program, we implemented both techniques, which we refer to as the package and photon modes, respectively.

The bioluminescent photon emission rate varies depending on the cell; the rate is in the range of 5–100 photons/cell/s.<sup>21</sup> The number of cells of a biolumi-

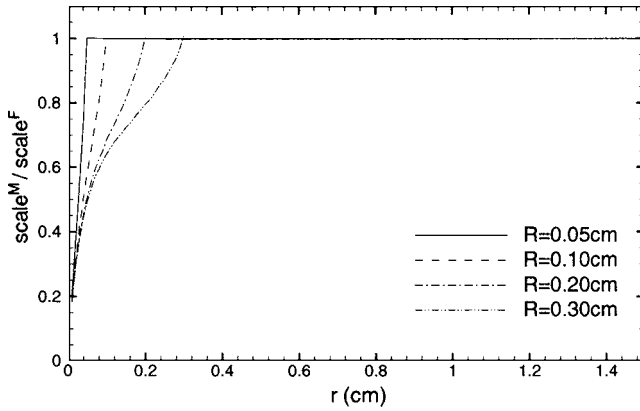


Fig. 7. Comparison of  $\text{scale}^M$  and  $\text{scale}^F$  with  $R = \{0.05, 0.1, 0.2, 0.3\}$  cm,  $\mu_a = 0.5$ ,  $\mu_s = 150$ , and  $g = 0.9$ . This figure shows that if  $r > R$ ,  $\text{scale}^M \approx \text{scale}^F$ .

nescent source for a small animal can be several millions. The power of the bioluminescent source is determined by the photon emission rate and the number of cells in the bioluminescent source. The power can be several thousand photons to several  $10^8$  photons. From the Eqs. (1)–(5), the result is in direct proportion to the power of the light source; hence we can use one source power in all simulations and still get the result for the other source power. Since the source power is decided by the number of cells, if we are using a ball source model,  $R$  has a relation with the cell type and the power of the source. Typically, an animal cell is about the size of  $10 \mu\text{m}$ ; then a  $R=1$  ball can contain approximately several  $10^6$  cells. A bioluminescent source can contain several thousand to  $10^7$  cells; hence  $R$  can be a submillimeter to several millimeters. In our study, we will use  $R = \{0.05, 0.1, 0.2, 0.3\}$  cm. In all our Monte Carlo simulation

experiments, we assumed  $P = 3 \times 10^7$  photons/s. We ran each test ten times with different random seeds and used the average as our result. In all the following figures,  $\text{MC}_P^F$  denotes the Monte Carlo result for Eq. (1),  $\text{MC}_P^M$  denotes the Monte Carlo result for testing Eq. (4) with  $\omega = \pi/2$  and  $\sigma = 0$ ,  $\text{MC}_B^F$  represents the Monte Carlo result for Eq. (2), and  $\text{MC}_B^M$  shows the Monte Carlo result for Eq. (5) with  $\omega = \pi/2$  and  $\sigma = 0$ . From the literature<sup>19,20,32</sup> the common range of  $\mu_a$  is  $[0.1, 1] \text{ cm}^{-1}$  and  $\mu_s$  is 100 to several hundred  $\text{cm}^{-1}$ . In this study, we use  $\mu_a = \{0.5, 1\}$ ,  $\mu_s = \{150, 250\}$ , and  $g = 0.9$ .

Figure 3 shows the comparison between  $\text{MC}_P^F$  and  $\phi_P^F$  [Eq. (1)] for combinations of different coefficients. For  $\mu_a = \{0.5, 1\}$ , the scale  $\text{MC}_P^F$  and  $\phi_P^F$  is very close to 1. Let us define the region with a less than 10% error as a good region, “GRegion.” For  $\mu_a = \{0.5, 1\}$ , the GRegion covers all the regions we are interested in, even when the detector is very close to the light source. Also, if  $\mu_s$  is increasing or  $\mu_a$  is decreasing, the diffusion approximation produces better results. Figure 4 examines  $\text{MC}_P^M$  and  $\phi_P^M$  [Eq. (4)]. It can be seen that the profiles in Fig. 4 are similar to those in Fig. 3. For Eq. (4), if the fiber is very close to the light source, the error is large, but the curve rapidly converges to almost 1.

Figure 5 compares  $\phi_B^F$  [Eq. (2)] with  $\text{MC}_B^F$  and  $\phi_B^M$  [Eq. (5)] with  $\text{MC}_B^M$  for a ball source. In this figure,  $\mu_a = 0.5$  and  $\mu_s' = 15$ , and  $R = \{0.05, 0.1, 0.2, 0.3\}$  cm. It is clear that there is a transition across the surface of the ball source. For  $r \geq R$ , the diffusion results are generally very good. For  $r < R$ , the error due to the diffusion approximation is not large if  $R$  is greater than 2 mm.

Figure 6 quantifies the difference between the Monte Carlo simulations between point and ball sources. Let  $\text{scale}^F = \phi_B^F / \phi_P^F$ . Then, we have

$$\text{scale}^F = \frac{\phi_B^F}{\phi_P^F} = \begin{cases} \frac{3[(e^{-R\mu_{\text{eff}}} - e^{R\mu_{\text{eff}}}) + R\mu_{\text{eff}}(e^{-R\mu_{\text{eff}}} + e^{R\mu_{\text{eff}}})]}{2R^3\mu_{\text{eff}}^3}, & r \geq R \\ \frac{3e^{-R\mu_{\text{eff}}}\{1 - e^{2r\mu_{\text{eff}}} + [2e^{(r+R)\mu_{\text{eff}}}r + R - e^{2r\mu_{\text{eff}}}R]\mu_{\text{eff}}\}}{2R^3\mu_{\text{eff}}^3}, & r < R \end{cases} \quad (7)$$

It can be seen that the diffusion prediction fits the simulation results fairly well, as shown from Figs. 6(a) and 6(c). Figure 6(a) shows that while  $r > R$ ,  $\text{MC}_B^F/\text{MC}_P^F$  is a constant. Figure 6(c) shows that while  $r > R$ , the diffusion prediction  $\text{scale}^F$  is a good estimation of  $\text{MC}_B^F/\text{MC}_P^F$ . Note that when  $R$  is large (for example, 2 mm), even if  $r \gg R$ , the equality  $\text{MC}_B^F \approx \text{MC}_P^F$  does not hold. Let us define  $\text{scale}^M = \phi_B^M / \phi_P^M$ . Figure 6(b) shows that while  $r > R$ ,  $\text{MC}_B^M/\text{MC}_P^M$  is a constant. Figure 6(d) shows that while  $r > R$ , the diffusion prediction  $\text{scale}^M$  is a good estimation of  $\text{MC}_B^M/\text{MC}_P^M$ . Figure 7 compares  $\text{scale}^M$  and  $\text{scale}^F$ , showing that for  $r > R$ , the two ratios are nearly identical. Based on these, an approximate version of Eq. (5) is given as follows:

$$\phi_{B,r \geq R}^M(\hat{r}, \hat{u}, \omega, R) = \phi_P^M(\hat{r}, \hat{u}, \omega) \frac{3[(e^{-R\mu_{\text{eff}}} - e^{R\mu_{\text{eff}}}) + R\mu_{\text{eff}}(e^{-R\mu_{\text{eff}}} + e^{R\mu_{\text{eff}}})]}{2R^3\mu_{\text{eff}}^3}. \quad (8)$$

#### 4. DISCUSSION AND CONCLUSION

We know the mean free path of a photon is  $1/(\mu_s + \mu_a)$ ; after each step, a photon can be absorbed or scattered or nothing happens. If  $\mu_s$  increases, the mean free path will decrease. For a point source, photons are launched at the

same location with a different direction. After photons are launched, the direction of the photon is leaving the light source. Since  $g=0.9$ , the photons need some scattering steps to be totally diffused. This is the reason why a diffusion equation has a relative large error while it is near a point source and increasing  $\mu_s$  will decrease the distance to diffuse the light source. For a ball source, the situation is different. For a point inside a ball source, the directions of launched photons around the point have all kinds of directions; hence for the point inside a ball source, the photons are already diffused by the volume of the ball source. For this reason, if the size of the ball source is large enough, the diffusion formula can have very accurate results even inside the ball source.

A strange phenomenon is while the distance is increasing,  $MC_B^F/MC_P^F \approx MC_B^M/MC_P^M = C$ , where  $C > 1$  is a constant. This means if  $R$  is large enough, we could not use a point source to model a ball source even if  $r$  is very large.

One important phenomenon we can see from Fig. 3 is that when the distance between the detector and the source is increased, the relative variation in the Monte Carlo simulation results is also increased. This is reasonable. The signal has an inherent Poisson noise<sup>33</sup>; when the signal is weak, the Poisson noise is relatively strong. For a Poisson distribution,  $\delta = \sqrt{\mu}$ , where  $\delta$  is the standard deviation and  $\mu$  is the mean value. In our COB configuration, we use a single-photon counter (SPCM16, PerkinElmer, Inc.) to count the number of photons. Let  $t$  be the counting time in seconds,  $N$  the number of photons incident on the detector in 1 s,  $Q$  the quantum efficiency, and  $D$  the dark count of the photon counter. The total readout of the photon counter is  $N \times t \times Q + D \times t$ ; hence the signal-to-noise ratio is  $N \times t \times Q / \sqrt{N \times t \times Q + D \times t}$ . The SPCM16 photon counter has a dark count of  $\sim 10/s$  and 65% quantum efficiency. To increase the signal-to-noise ratio, increasing  $t$  is the only choice.

In conclusion, we have formulated solutions for photon fluence and detector measurement based on the diffusion approximation in the cases of point and ball sources. Then, we have evaluated those formulas against the Monte Carlo simulation. Our results have indicated the following guidelines for COB:

(a) If  $\mu'_s \gg \mu_a$  and  $r$  is large (1 mm in most cases), the diffusion equation is a good approximation with a  $< 10\%$  error.

(b) If  $\mu_a$  is large, the diffusion approximation can apply only within a narrow region. A Monte Carlo simulation can be conducted to delimit the region.

(c) Equation (5) is a good approximation of the Monte Carlo simulation.

(d) For a ball source with  $R \leq 1$  mm, we can use a point source model without any correction for  $r \geq R$ .

(e) For a ball source with large  $R$ , we can use a point source to approximate a ball source according to Eq. (8) for  $r \geq R$ .

## ACKNOWLEDGMENT

This work is supported in part by the National Institutes of Health/National Institute of Biomedical Imaging and Bioengineering grant EB001685.

H. Shen's e-mail address is haiou-shen@uiowa.edu.

## REFERENCES

1. G. Wang, E. Hoffman, G. McLennan, L. Wang, M. Suter, and J. Meinel, "Development of the first bioluminescent CT scanner," *Radiology* **229**, 566 (2003).
2. W. Cong, G. Wang, D. Kumar, Y. Liu, M. Jiang, L. Wang, E. Hoffman, G. McLennan, P. McCray, J. Zabner, and A. Cong, "A practical reconstruction method for bioluminescence tomography," *Opt. Express* **13**, 6756–6771 (2005).
3. W. Cong, D. Kumar, Y. Liu, A. Cong, and G. Wang, "A practical method to determine the light source distribution in bioluminescent imaging," in *Proc. SPIE* **5535**, 679–686 (2004).
4. G. Wang, Y. Li, and M. Jiang, "Uniqueness theorems in bioluminescence tomography," *Med. Phys.* **31**, 2289–2299 (2004).
5. M. Jiang and G. Wang, "Image reconstruction for bioluminescence tomography," in *Proc. SPIE* **5535**, 335–351 (2004).
6. V. Ntziachristos, C. Bremer, and R. Weissleder, "Fluorescence imaging with near-infrared light: new technological advances that enable in vivo molecular imaging," *Eur. Radiol.* **13**, 195–208 (2003).
7. G. Wang, Y. Li, and M. Jiang, "Computational optical biopsy methods, techniques and apparatus," patent disclosure filed with the University of Iowa Research Foundation in December 2003; provisional patent filed in 2004.
8. Y. Li, M. Jiang, and G. Wang, "Computational optical biopsy," *Biomed. Eng. Online* **4**:36 (2005).
9. S. Chandrasekhar, *Radiative Transfer* (Clarendon, 1950).
10. K. Case and P. Zweifel, *Linear Transport Theory* (Addison-Wesley, 1967).
11. A. Ishimaru, *Wave Propagation and Scattering in Random Media* (Academic, 1978).
12. E. Shettle and J. Weinman, "The transfer of solar irradiance through inhomogeneous turbid atmospheres evaluated by Eddington's approximation," *J. Atmos. Sci.* **27**, 1048–1055 (1970).
13. J. Joseph, W. Wiscombe, and J. Weinman, "The delta-Eddington approximation for radiative flux transfer," *J. Atmos. Sci.* **33**, 2452–2459 (1976).
14. S. Prahl, "Light transport in tissue," Ph.D. dissertation (University of Texas at Austin, 1988).
15. D. Boas, "Diffuse photon probes of structural and dynamical properties of turbid media," Ph.D. dissertation (University of Pennsylvania, 1996).
16. R. Groenhuis, H. Ferwada, and J. T. Bosch, "Scattering and absorption of turbid materials determined from reflection measurements. 1. Theory," *Appl. Opt.* **22**, 2456–2462 (1983).
17. M. Schweiger, S. Arridge, M. Hiraoka, and D. Delpy, "The finite element method for the propagation of light in scattering media: boundary and source conditions," *Med. Phys.* **22**, 1779–1792 (1995).
18. E. Aydin, C. Oliveira, and A. J. H. Goddard, "A comparison between transport and diffusion calculations using a finite element-spherical harmonics radiation transport method," *Med. Phys.* **29**, 2013–2023 (2002).
19. W. Cheong, S. Prahl, and A. J. Welch, "A review of the optical properties of biological tissues," *IEEE J. Quantum Electron.* **26**, 2166–2184 (1990).
20. V. Tuchin, *Tissue Optics: Light Scattering Methods and Instruments for Medical Diagnosis* (SPIE, 2000).
21. B. Rice, M. Cable, and M. Nelson, "In vivo imaging of light emitting probes," *J. Biomed. Opt.* **6**, 432–440 (2001).
22. S. Flock, M. Patterson, B. Wilson, and D. Wyman, "Monte Carlo modeling of light propagation in highly scattering tissues-I: model predictions and comparison with diffusion theory," *IEEE Trans. Biomed. Eng.* **36**, 1162–1168 (1989).
23. I. Manno, *Introduction to the Monte Carlo Method* (Akadémiai Kiadó, 1999).

24. W. Cong, L. Wang, and G. Wang, "Formulation of photon diffusion from spherical bioluminescent sources in an infinite homogeneous medium," *Biomed. Eng. Online* **3**:12 (2004).
25. R. Haskell, L. Svaasand, T. Tsay, T. Feng, M. McAdams, and B. Tormberg, "Boundary conditions for the diffusion equation in radiative transfer," *J. Opt. Soc. Am. A* **11**, 2727–2741 (1994).
26. B. Wilson and G. Adam, "A Monte Carlo model for the absorption and flux distributions of light in tissue," *Med. Phys.* **10**, 824–830 (1983).
27. S. Prahl, M. Keijzer, S. Jacques, and A. Welch, "A Monte Carlo model of light propagation in tissue," in *Proc. SPIE* **5**, 102–111 (1989).
28. S. Flock, B. Wilson, and M. Patterson, "Monte Carlo modeling of light propagation in highly scattering tissues—II: comparison with measurements in phantoms," *IEEE Trans. Biomed. Eng.* **36**, 1169–1173 (1989).
29. L. Wang, S. Jacques, and L. Zheng, "MCML—Monte Carlo modeling of photon transport in multi-layered tissues," *Comput. Methods Programs Biomed.* **47**, 131–146 (1995).
30. H. Li, J. Tian, F. Zhu, W. Cong, L. Wang, E. Hoffman, and G. Wang, "A mouse optical simulation environment (MOSE) to investigate bioluminescent phenomena with the Monte Carlo method," *Acad. Radiol.* **11**, 1029–1038 (2004).
31. S. Jacques, "Light distributions from point, line, and plane sources for photochemical reactions and fluorescence in turbid biological tissues," *Photochem. Photobiol.* **67**, 23–32 (1998).
32. B. C. Wilson, "Measurement of tissue optical properties: methods and theories," in *Optical-Thermal Response of Laser-Irradiated Tissue*, A. J. Welch and M. J. C. van Gemert, eds. (Plenum, 1995).
33. S. Arridge, M. Hiraoka, and M. Schweiger, "Statistical basis for the determination of optical path length in tissue," *Phys. Med. Biol.* **40**, 1539–1558 (1995).